

Importance of Melt Flow in Solidifying Mushy Zone

M. Wu*, A. Vakhrushev, G. Nummer, C. Pfeiler, A. Kharicha and A. Ludwig

Simulation and Modeling of Metallurgical Processes, Department of Metallurgy, University of Leoben, A-8700 Leoben, Austria

Abstract: A mixture solidification model is employed to study the interaction between the melt flow and the growing mushy zone. The goal is to address the importance of considering the melt flow and flow pattern (laminar or turbulent) in the growing mushy zone. A simple 2D benchmark with parallel flow passing by/through a vertically growing mushy zone is considered. Parameter studies with different velocities and flow patterns are performed. It is found that the flow velocity and flow pattern in and near the mushy zone plays an extremely important role in the formation of the mushy zone. The mushy zone thickness is dramatically reduced with the increasing melt velocity. Simulations with/without considering turbulence show significantly different results. The turbulence in the mushy zone is currently modeled with a simple assumption that the turbulence kinetic energy is linearly reduced with the mush permeability.

Keywords: Modeling, solidification, mushy zone, permeability, turbulence.

1. INTRODUCTION

Solidification is a key issue for many industry processes such as casting, welding, crystal growth, metallurgy, energy conservation, refrigeration, polymer crystallization. Most industry materials solidify in a temperature interval, and they subject a phase transition from purely liquid state, through a liquid-solid two phase region which is also called as mushy zone, to a complete solid state. Flow in the mushy zone plays an important role in the final solidified microstructure. In last decades many experimental and numerical studies have been carried out for the solidification of metal materials. Some numerical models have been developed to account for both fluid flow and heat transfer, and incorporate with solidification kinetics as well [1, 2]. However, the knowledge about the influence of the flow on the developing mushy zone is quite limited, especially when it is exposed to a melt region with highly turbulent flow. Most recent solidification models incorporate only with laminar flow [3-6]. Only few works were reported to handle the turbulence during solidification [7-10].

In the current paper an existing model [7-10] is employed to study the interaction between the flow and the mushy zone. A simple 2D benchmark with parallel flow passing by/through a vertically growing mushy zone is configured. Parameter studies with different flow patterns and flow parameters are performed.

2. NUMERICAL MODEL

A mixture continuum [3-6] is used to mimic the mushy zone (Fig. 1). This mixture combines liquid ℓ -phase and

solid s-phase, which are quantified by their volume fractions, f_ℓ and f_s . The morphology of the solid phase is usually dendritic, but here we consider the dendritic solid phase as a part of the mixture continuum. The mixture continuum changes continuously from a pure liquid region, through the mushy zone (two phase region), to the complete solid region. The evolution of the solid phase is determined by the temperature according to a $f_s - T$ relation (e.g. Gulliver-Scheil),

$$f_s = \begin{cases} 0 & T > T_{\text{liquidus}} \\ 1 - \left((T_f - T) / (T_f - T_{\text{liquidus}}) \right)^{\frac{1}{k_p - 1}} & T_{\text{liquidus}} \geq T > T_{\text{Eutectic}} \\ 1 & T_{\text{Eutectic}} \geq T. \end{cases} \quad (1)$$

Only one set of Navier-Stokes equation, which applies to the domain of the bulk melt and mushy zone, is solved in the Eulerian frame of reference.

$$\nabla \cdot \bar{u} = 0, \quad (2)$$

$$\rho \frac{\partial \bar{u}}{\partial t} + \rho \nabla \cdot (\bar{u} \otimes \bar{u}) = -\nabla p + \nabla(\mu_{\text{eff}} \nabla \cdot \bar{u}) + \rho \bar{g} + \bar{S}_{\text{mon}}, \quad (3)$$

$$\text{where } \bar{u} = \begin{cases} \bar{u}_\ell & \text{bulk melt region} \\ f_\ell \bar{u}_\ell + f_s \bar{u}_s & \text{mushy zone} \\ \bar{u}_s & \text{solid region.} \end{cases} \quad (4)$$

Here \bar{u}_s is the pre-described velocity of the solid phase. The momentum sink due to the drag of the solid dendrites in the mushy zone is modeled by the Blake-Kozeny law:

$$\bar{S}_{\text{mon}} = -\frac{\mu_\ell}{K} \cdot (\bar{u} - \bar{u}_s) \quad (5)$$

The permeability for steel, for example, is modeled as function of the volume fraction and the primary dendrite arm spacing λ_1 according to Gu and Beckermann [11]:

*Address correspondence to this author at the Simulation and Modeling of Metallurgical Processes, Department of Metallurgy, University of Leoben, A-8700 Leoben, Austria; Tel: 0043-3842-4023103; Fax: 0043-3842-4023102; E-mail: menghuai.wu@mu-leoben.at

$$K = \frac{f_\ell^3}{f_s^2} \cdot 6 \cdot 10^{-4} \cdot \lambda_l^2 . \quad (6)$$

The energy equation is applied to the entire domain,

$$\rho \frac{\partial h}{\partial t} + \rho \nabla \cdot (\bar{u}h) = \nabla \cdot \lambda_{\text{eff}} \nabla T + S_e . \quad (7)$$

Here h is the sensitive enthalpy of the solid phase $h_s = h_{\text{ref}} + \int_{T_{\text{ref}}}^T c_p dT$. The latent heat released, L , is treated by a source term

$$S_e = \rho L \partial f_s / \partial t + \rho L \bar{u}_s \cdot \nabla f_s . \quad (8)$$

A low Reynolds number $k - \varepsilon$ model was introduced by Prescott and Incropera [7-10] to handle the turbulence during solidification.

$$\frac{\partial(\rho k)}{\partial t} + \nabla \cdot (\rho \bar{u}k) = \nabla \cdot \left(\left(\mu_\ell + \frac{\mu_t}{\text{Pr}_{t,k}} \right) \nabla k \right) + G - \rho \varepsilon + S_k , \quad (9)$$

$$\frac{\partial(\rho \varepsilon)}{\partial t} + \nabla \cdot (\rho \bar{u} \varepsilon) = \nabla \cdot \left(\left(\mu_\ell + \frac{\mu_t}{\text{Pr}_{t,\varepsilon}} \right) \nabla \varepsilon \right) + C_{1\varepsilon} G \frac{\varepsilon}{k} - C_{2\varepsilon} \rho \frac{\varepsilon^2}{k} , \quad (10)$$

where $S_k = -\frac{\mu_\ell}{K} \cdot k$.

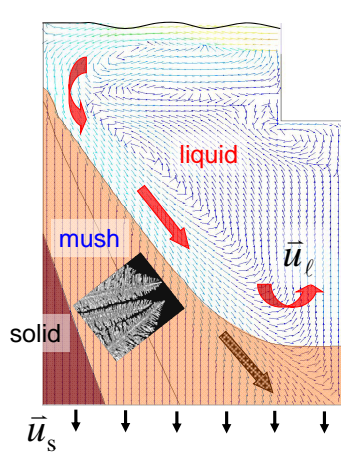


Fig. (1). Schematic of the two-phase nature of a solidifying mushy zone.

The turbulent Prandtl numbers for $k : \text{Pr}_{t,k} = 1.0$, and for $\varepsilon : \text{Pr}_{t,\varepsilon} = 1.3$. G is the shear production of turbulence kinetic energy [7-10]. A simple approach is used to modify the turbulence kinetic energy in the domain which may include a mushy zone. It is assumed that within a coherent mushy zone turbulence is damped by shear which is linearly correlated with the reduction of the mush permeability. The influence of turbulence (standard $k - \varepsilon$ model) on the momentum and energy transports are considered by the effective viscosity $\mu_{\text{eff}} = \mu_\ell + \mu_t$ and the effective thermal conductivity $\lambda_{\text{eff}} = \lambda + \lambda_t$, where $\mu_t = \rho C_\mu k^2 / \varepsilon$, $\lambda_t = f_\ell \mu_t c_{p,\ell} / \text{Pr}_{t,h}$, C_μ is a model parameter (0.09), $\text{Pr}_{t,h}$ is the turbulent Prandtl number for energy equation (0.85).

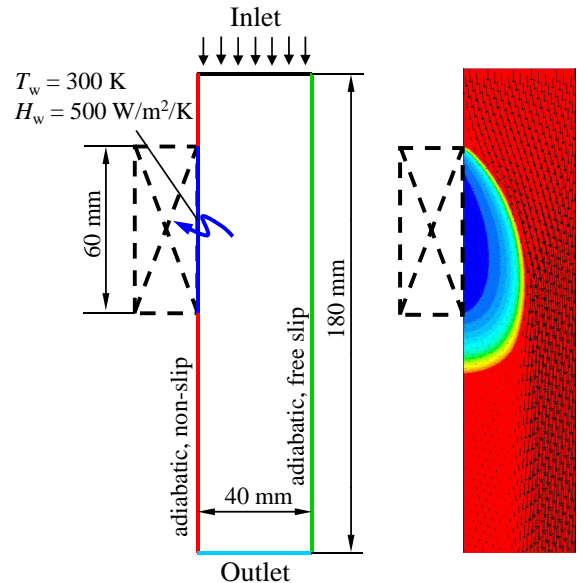


Fig. (2). Configuration of the benchmark: (left) geometry and boundary conditions; (right) schematic of the flow in the calculation domain and the mushy zone developed in front of the chill-wall. The solid phase is stationary.

Table 1. Parameters used for the Calculations (Fe-0.34 wt.%C)*

Thermal Physical Properties	Thermal Dynamical Data
$c_p = 808.25 \text{ J} \cdot \text{kg} \cdot \text{K}^{-1}$	$k_p = 0.2894 \text{ -}$
$\lambda = 33.94 \text{ W} \cdot \text{m}^{-1} \cdot \text{K}^{-1}$	$m = -8453.0 \text{ K}$
$\rho = 7027 \text{ kg} \cdot \text{m}^{-3}$	$T_f = 1811 \text{ K}$
$\mu_\ell = 5.6 \times 10^{-3} \text{ kg} \cdot \text{m}^{-1} \cdot \text{s}^{-1}$	$T_e = 1426 \text{ K}$
$L = 256,476.0 \text{ J} \cdot \text{kg}^{-1}$	$c_e = 0.043 \text{ -}$
	$T_{\text{liquidus}} = 1782 \text{ K}$
Other parameters	
$\lambda_l = 4 \cdot 10^{-4} \text{ m}$	
$T_{\text{inlet}} = 1785 \text{ K}$	
$\bar{u}_{\text{inlet}} = 0.001 \text{ m} \cdot \text{s}^{-1}$ (later varied)	

* Some modeling parameters were described in section 2.

3. BENCHMARK SIMULATIONS

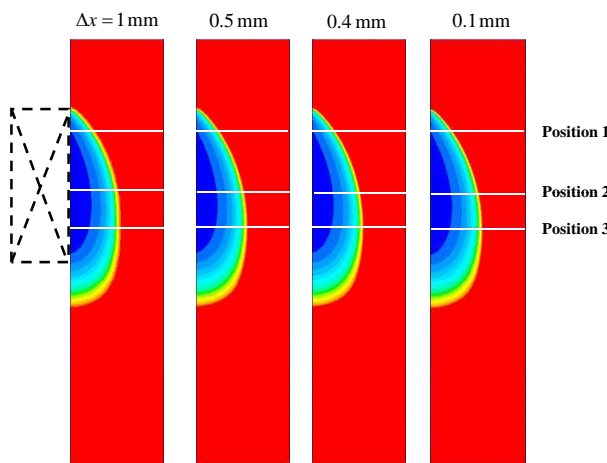
A 2D benchmark, as shown in Fig. (2), is considered. The melt with nominal composition of Fe-0.34wt.%C fills continuously through the inlet into the domain with constant temperature (1785 K) and constant velocity ($\bar{u}_{\text{inlet}} = 0.01 \text{ m} \cdot \text{s}^{-1}$). The mold is adiabatic, except that a chill is placed on the left side of the mold to cool the melt. Solidification occurs in front of the chill, and the solid phase is assumed to be stationary, and it sticks (non-slip) to chill surface. The melt passes by or through, and interacts with the solidifying mushy zone, and finally leaves the domain from the outlet. Turbulence boundary conditions at the

mold walls are: zero of k , zero flux of ε . At the inlet, the k and ε are estimated based on the given turbulence intensity I and hydraulic diameter D_H : $k_{\text{inlet}} = (\bar{u}_{\text{inlet}} | I)^2 \cdot 3/2$, $\varepsilon_{\text{inlet}} = C_{\mu}^{3/4} \cdot k_{\text{inlet}}^{3/2} / 0.07D_H$. Other boundary conditions, thermal physical properties and thermal dynamical data are given in Fig. (2) and Table 1.

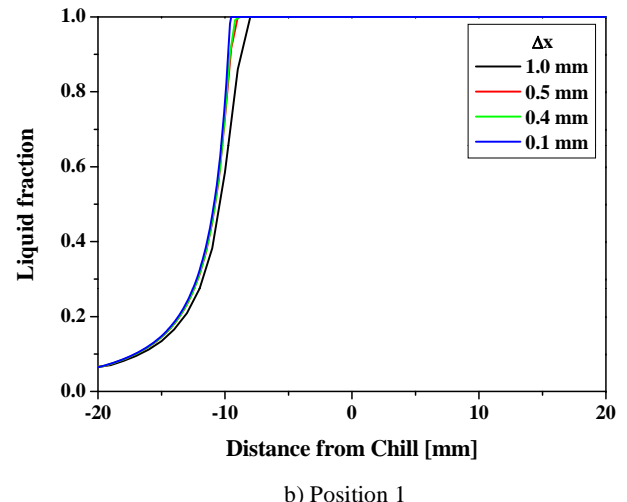
3.1. Mesh Dependency Analysis

To verify the calculation accuracy, mesh dependency of the simulation result was studied. The calculation domain is enmeshed with structured (square) mesh. 4 different mesh sizes are used: $\Delta x = 1, 0.5, 0.4, 0.1 mm. All simulations are made with constant inlet velocity $\bar{u}_{\text{inlet}} = 0.01$ m·s⁻¹, and constant inlet temperature $T_{\text{inlet}} = 1785$ K. Only laminar flow model is considered for this study. The k - ε model is$

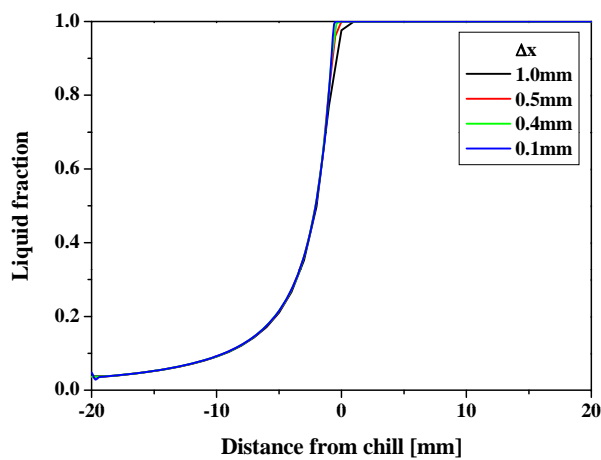
switched off. Fig. (3a) compares the steady-state results of the mushy zone for the 4 different mesh sizes. Varying the mesh size from 0.1 to 1.0 mm, almost no significant influence on the mushy zone is seen. If we study the liquid fraction distribution across different sections carefully (3 sections as indicated in Fig. (3a), position 1 - 3), only minor difference is seen (Fig. 3b-d). The results with $\Delta x = 0.5, 0.4, 0.1 mm are almost imposed with each other, which are slightly different from the results with $\Delta x = 1 mm. The relatively large discrepancy is located near the front region of the mushy zone. We can claim that the results with Δx smaller than 0.5 mm can be accepted as grid independent result. With further refinement of the grid size would increase the calculation cost, but no significant improvement of the accuracy. Note that the criterion ($\Delta x < 0.5 mm) may not apply generally. When the process conditions change, for$$$



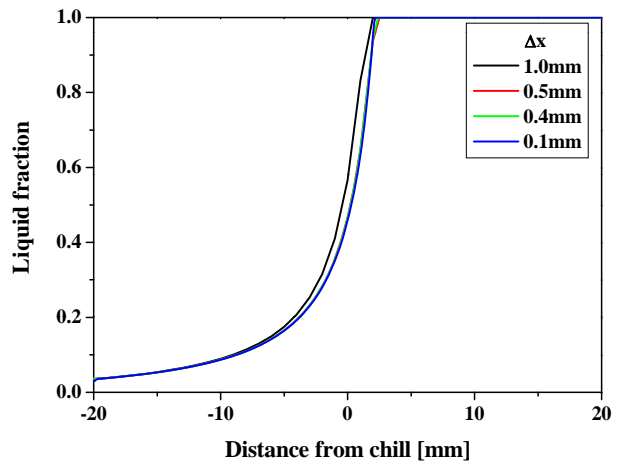
a) overview of 4 cases



b) Position 1



c) Position 2



d) Position 3

Fig. (3). Sensitivity of the simulation results to the mesh size. 4 simulations with different mesh sizes (0.1, 0.4, 0.5, 1 mm) are performed. **a)** Overview of the mushy zones of the 4 cases: red indicating the bulk melt region, blue indicating the solid region, and other colors indicating the mushy zone; **b-d)** Volume fraction distribution of the liquid phase across the section at Position 1, 2, 3.

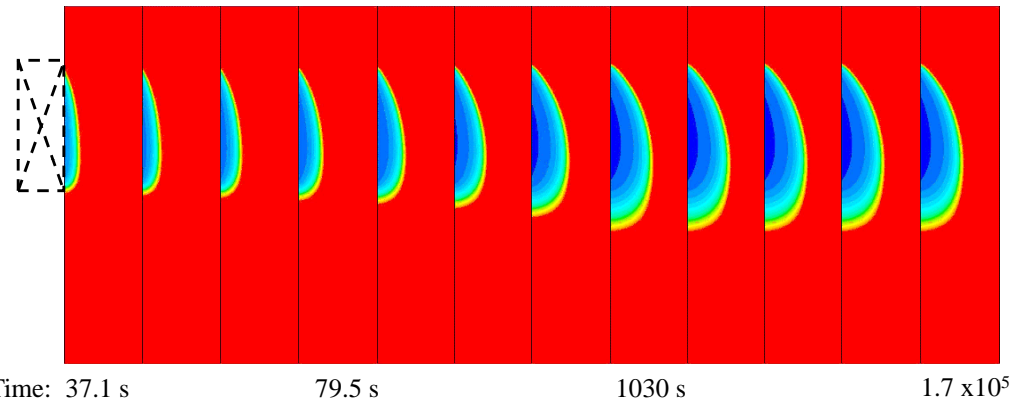


Fig. (4). Evolution of the mushy zone from the initial condition of full melt of $T_0 = 1785$ K. During the process the inlet velocity and inlet temperature are kept constant: $\bar{u}_{\text{inlet}} = 0.01$ m·s $^{-1}$, $T_{\text{inlet}} = 1785$ K. Volume fraction of the liquid phase is color-scaled: red indicating the bulk melt region, blue indicating the solid region, and other colors indicating the mushy zone.

example, the melt velocity increases finer grid would be required. Therefore, for each process condition the similar grid indecency proofs should be performed.

3.2. Evolution of the Mushy Zone

A transient simulation result of the mushy zone is shown in Fig. (4). We have used a dynamic time step control. We start the calculation with an initial time step of 10^{-4} s. In each time step a limit of iteration number (100) is set. The calculation iterations are carried out until the convergent criteria (residual for continuity and momentum equations are 10^{-5} , and for energy equation is 10^{-8}) are reached. When the iteration number required to reach the convergent criteria is smaller than 30, the time step is increased by a factor of 20%. When the iteration number required is larger than 50, the time step is reduced by a factor of 20%. When the maximum iteration number 100 is required without reaching the convergent criteria, the time step is reduced by a factor of 20%, and the calculation is switched to the next time step. With this strategy a relative safe and convergent result in each time step can be ensured. The simulation does show sensitivity to the time step, when the first layer of the solid phase forms near the chill surface. Due to the initial high cooling rate, the solidification rate at the chill surface region is very high. The high solidification rate leads to the high rate of the latent heat release, which causes the solution instability of the energy equation.

As shown in Fig. (4), The whole process proceeds to about ca. 1000 s until mushy zone reaches the steady state. Due to the continuous flow, the developing mushy zone becomes stable afterwards. It means that the rate of heat extraction by the chill is balanced by the energy loss of the melt when passing through the domain.

Fig. (5) shows details of the flow near and in the mushy zone. The flow can only penetrate into the mush as deep as $f_s = 20\text{-}30\%$. As expressed in Eq. (6) the permeability of the mushy zone drops dramatically with the increase of f_s . The permeability is a function of the primary dendrite arm space

(PDAS). If the PDAS is large, the permeability is high, and the melt will easily penetrate deep into the mush. The shape of the mushy zone shows that the area which face the flow (upper region) the mushy zone is thinner because of the strong flow entering the mushy zone. In the downstream area the mushy zone is much thicker, because the flow is hindered/depressed by the mushy zone there.

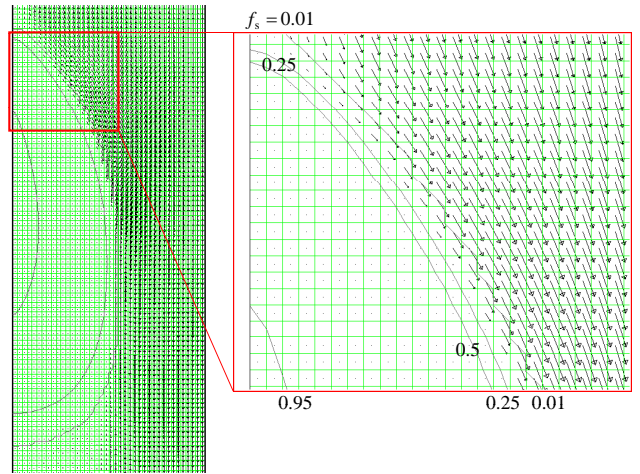


Fig. (5). Melt flow (vector of \bar{u}_t) near and in the mushy zone. The inlet velocity and temperature are kept constant: $\bar{u}_{\text{inlet}} = 0.01$ m·s $^{-1}$, $T_{\text{inlet}} = 1785$ K. Here only the laminar flow is considered, and the final steady state result is analyzed. The solid fraction distribution is shown with isolines.

3.3. Influence of the Velocity on the Mush Thickness

Influence of the flow velocity on the mush thickness is studied by varying the inlet velocity. 4 inlet velocities are considered (Fig. 6). The estimated Reynolds numbers of the 4 cases are 2500, 1500, 500, 50, correspondingly. We assume that the flow pattern is still laminar. In the case of high inlet velocity, e.g. 0.05 m·s $^{-1}$, only tiny layer of the mushy zone is seen. The high heat extraction rate of the chill is balanced by the high flow rate of the melt. The mush thickness

increases with the decreasing inlet velocity. As shown in Fig. (6), when the inlet velocity is reduced to $0.001 \text{ m}\cdot\text{s}^{-1}$, the mush thickness is extended to most of the sample section. The flow channel in front of the mushy zone becomes narrow. Due to the constant inlet velocity condition, the velocity in the channel increases with the decrease of the channel section. However, the channel will never be closed by the mushy zone. The heat transfer rate through the mushy zone into the chill will be balanced by the increasing melt flow rate in the narrowing channel.

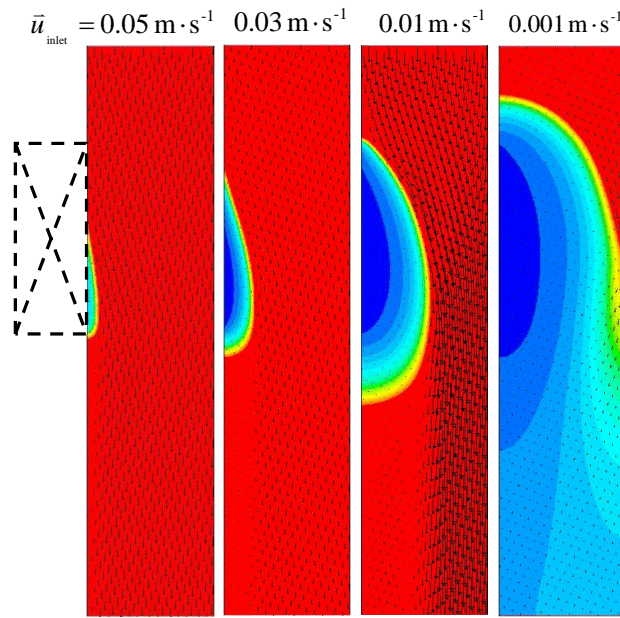


Fig. (6). Influence of the inlet velocity on the mush thickness. The inlet temperature is kept constant: $T_{\text{inlet}} = 1785 \text{ K}$. Here only the laminar flow pattern is considered, and steady state results are analyzed.

3.4. Influence of the Turbulence on the Mush Thickness

The influence of the turbulence on the mushy zone is significant. Two simulations without and with considering the turbulence model are compared in Fig. (7a and b). With considering the turbulence, the mush thickness is predicted significantly smaller. The assumption of laminar flow applies in most region of the calculation domain, but it does not apply in the whole domain, as shown by Fig. (7c-d). The calculated k and ε in the most bulk region are neglect small, but in the front of or near the front of the mushy zone, and in the downstream region, they are significantly increased. Due to this fact, μ_{eff} is not equally distributed, and it is increased by a factor of 9 in some regions. In this sense, λ_{eff} is increased by a factor 2.4. As the solidification model, Eq. (1), stated, the mushy zone thickness is governed by the temperature field. If λ_{eff} is increased due to the effect of turbulence, the temperature gradient increases, the mushy zone becomes narrow.

To understand the influence of λ_{eff} on the mushy zone, additional test simulations with an artificially increased λ_{eff}

are performed (Fig. 8). The λ_{eff} is artificially increased by a factor of 2 and 3 uniformly in the entire calculation domain. The modeling results with the artificially increased λ_{eff} are compared with the reference case of pure laminar flow ($\lambda_{\text{eff}} = \lambda$). It is found that the mushy zone is dramatically reduced when λ_{eff} is doubled, and the mushy zone almost disappears when λ_{eff} is increased by a factor of 3. These simulations hint that the turbulence in the mush or near/in the front of the mushy zone can play extremely important role in the formation of the mushy zone. The simulation with turbulence model (Fig. 7) shows that k and ε are not uniformly distributed. They are obviously increased locally in some regions, e.g. near the front of the mushy zone, hence the effective thermal conductivity λ_{eff} is increased as well. Therefore, great care should be taken to account the turbulence effect, and its influence on the formation of the mushy zone.

4. SUMMARY DISCUSSIONS

The interactions between the melt flow and the mushy zone can be extremely complicated. As schematically shown in Fig. (9), whenever flow approaches mushy zone, dendrite tips may cause additional perturbation or instability of the flow on one hand, the turbulence inside the mushy zone (between the dendrite arms) will be damped by the mushy zone on the other hand. The influences of the flow on the mushy zone include: (1) modify the dendritic morphology, (2) induce macrosegregation, (3) cause segmentation, brunches and detachment of the dendrite arms, (4) influence the mushy zone thickness. In turn the influences of the mushy zone on the flow include: (1) modify the flow pattern (laminar or turbulence behavior), (2) induce or dampen the turbulence. There is no well-defined boundary layer in front of the mushy zone, and the thickness/position of the mushy zone is a part of solution which can not be pre-defined. This article can not cover all aspects of the aforementioned interactions. We focus currently on only one point, i.e. the influence of flow and flow pattern on the evolution of the mushy zone thickness, which is of ultimate importance for metallurgist to understand and control the formation of the solid shell in the continuous caster.

The mixture solidification model, used for the current study, has been verified theoretically and experimentally [3-8]. The current authors applied the same model to predict the evolution of the solid shell thickness of continuous cast steel slab [12, 13], and compared the prediction with the experiment on the breakout shell [14]. Good quantitative agreement between them was obtained. An improved model being able to properly incorporate the turbulence flow in/near progressing mushy zone is desirable. The modified standard k - ε model, suggested by Prescott and Incropera [9, 10], has provided a simple approach to treat the turbulence flow in the mushy region. The turbulence is simply assumed to be damped by the mushy zone. The turbulence kinetic energy is considered to be linearly reduced with the decrease of mush permeability. The numerical simulation

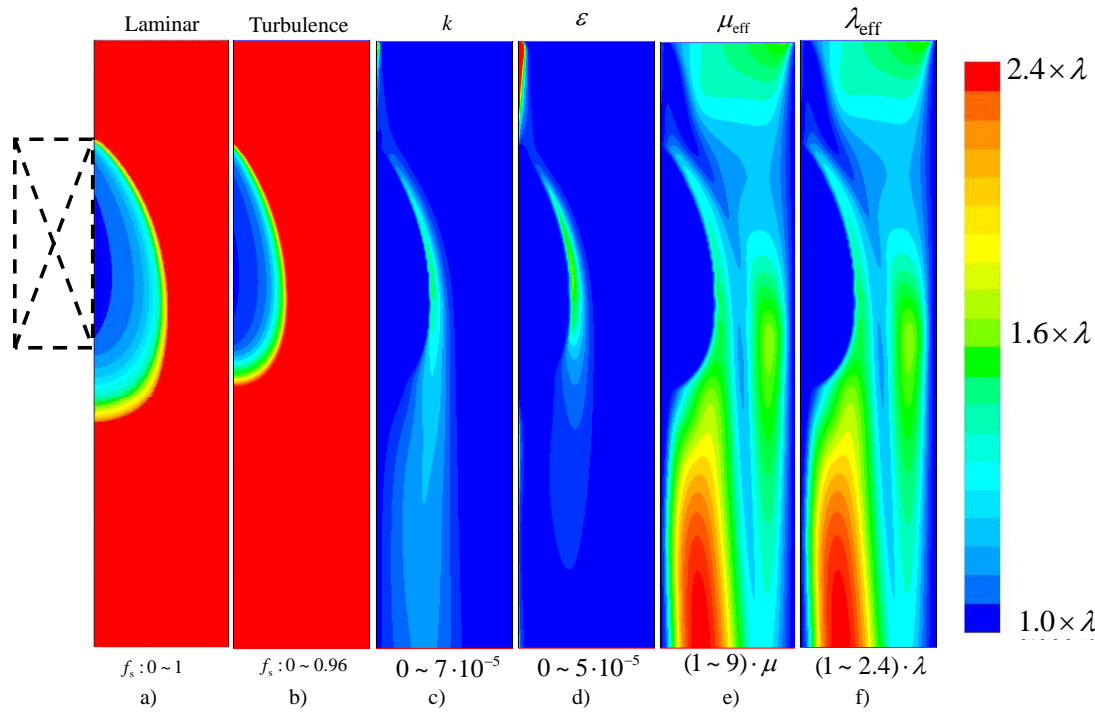


Fig. (7). Steady state mushy zone simulated without (a) and with (b) considering the turbulence model. (c) – (f) are the turbulence kinetic energy, dissipation rate, effective viscosity, and effective thermal conductivity in the case of considering turbulence model. The inlet velocity and temperature are constant: $\bar{u}_{\text{inlet}} = 0.01 \text{ m} \cdot \text{s}^{-1}$, $T_{\text{inlet}} = 1785 \text{ K}$. Inlet boundary conditions for k and ε are estimated based on the given hydraulic diameter $D_H = 0.04 \text{ m}$ and constant turbulence intensity $I = 0.07$ (root-mean-square of turbulence velocity fluctuation divided by mean velocity).

of a Pb-Sn casting has explored some interesting features of macrosegregation, which shows qualitative agreement with experiments. Considering the complexity of the solidification process, as schematically shown in Fig. (9), further modeling efforts, especially in the presence of turbulent flow in mushy region, and dedicated experimental evaluations are required. Some turbulence models were recently developed in the disciplinary of porous medium. For example, Nakayama and Kawahara have proposed a modified two-equation $k - \varepsilon$ model [15, 16] to consider the turbulence flow in porous medium by introducing two additional terms representing the production and dissipation rate of turbulence kinetic energy and its dissipation rate. Masuoka and Takatsu proposed an even simple zero-equation model [17] for flow in packed spherical particles based on the consideration of effective eddy diffusivity as the algebraic sum of the eddy diffusivities estimated from the pseudo vortex (order of particle diameter) and the interstitial vortex between the packed particles. Although the solidification mushy zone is generally characterized with its transient behaviour and non-homogeneity, it has some similarity to the porous medium. The ideas developed in the disciplinary of porous medium would certainly stimulate the future work to improve the turbulence model in the solidifying mushy zone.

The current paper has addressed the importance of the flow phenomena in the solidification process. Based on numerical parameter studies we found that the mushy zone thickness is dramatically reduced with the increase of flow

velocity. When the turbulence is considered, the thickness of the mushy zone becomes even further thinner. The general effect of the turbulence is to enhance the heat dispersion in the flow domain. The turbulence will enhance the local temperature gradient in/near the mushy region. According to the $f_s - T$ relation, Eq. (1), the larger the temperature gradient, the thinner the mushy zone.

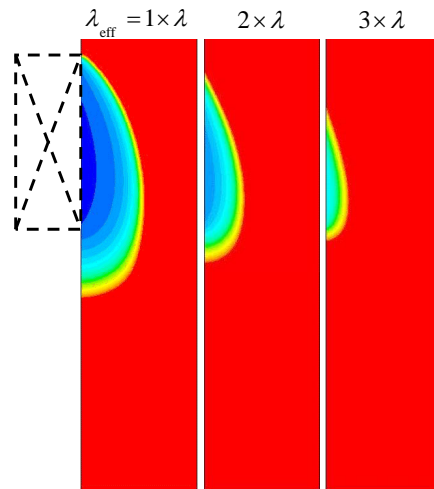


Fig. (8). Influence of the effective thermal conductivity on the mush thickness. Simulations with an artificially increased (effective) thermal conductivity were performed.

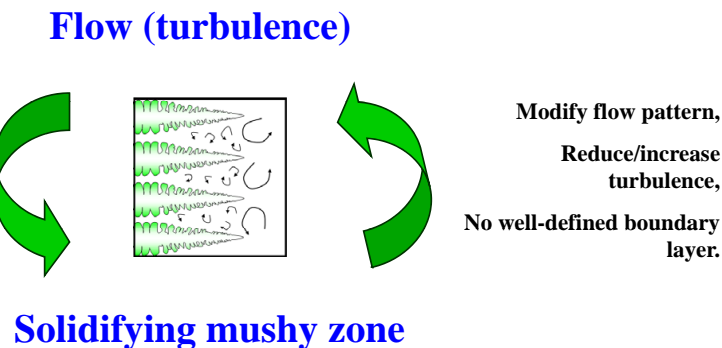


Fig. (9). Schematic of interactions between the melt flow and the mushy zone.

NOMENCLATURE

c_0	1	initial concentration
c_e	1	eutectic concentration
c_p	$\text{J} \cdot \text{kg}^{-1} \cdot \text{K}^{-1}$	specific heat
$C_{1\epsilon}, C_{2\epsilon}, C_\mu$	1	constant of the standard $k - \epsilon$ model [7-10]
D	m	characteristic length of the flow domain
D_H	m	hydraulic diameter of inlet
f_ℓ, f_s	1	volume fraction of liquid and solid phase
\bar{g}	$\text{m} \cdot \text{s}^{-2}$	gravity acceleration
G	$\text{kg} \cdot \text{m}^{-1} \cdot \text{s}^{-3}$	shear production of turbulence kinetic energy
h	$\text{J} \cdot \text{kg}^{-1}$	enthalpy
h_{ref}	$\text{J} \cdot \text{kg}^{-1}$	reference enthalpy at temperature T_{ref}
h_s	$\text{J} \cdot \text{kg}^{-1}$	enthalpy of solid phase
I	1	turbulence intensity
k	$\text{m}^2 \cdot \text{s}^{-2}$	turbulence kinetic energy per unit of mass
k_p	1	partition coefficient of binary alloy
K	m^2	permeability
L	$\text{J} \cdot \text{kg}^{-1}$	latent heat
m	K	liquidus slope of binary alloy
p	$\text{N} \cdot \text{m}^{-2}$	pressure
$\text{Pr}_{t,h}$	1	Prandtl number for energy equation
$\text{Pr}_{t,k}$	1	Prandtl number for turbulence kinetic energy k
$\text{Pr}_{t,\epsilon}$	1	Prandtl number for turbulence dissipation rate ϵ
R_e	1	Reynolds number
S_e	$\text{J} \cdot \text{m}^{-3} \cdot \text{s}^{-1}$	source term for energy equation
S_k	$\text{kg} \cdot \text{m}^{-1} \cdot \text{s}^{-3}$	source term for turbulence kinetic energy
\bar{S}_{mon}	$\text{kg} \cdot \text{m}^{-2} \cdot \text{s}^{-2}$	source term for momentum equation
t	s	time
T	K	temperature
T_{eutectic}	K	temperature of eutectic reaction
T_f	K	melt point of pure solvent
T_{inlet}	K	inlet temperature

NOMENCLATURE contd.....

T_{liquidus}	K	liquidus temperature of alloy
T_{ref}	K	reference temperature for h_{ref}
\bar{u}	$\text{m}\cdot\text{s}^{-1}$	velocity of the mixture
\bar{u}_{inlet}	$\text{m}\cdot\text{s}^{-1}$	inlet velocity
\bar{u}_ℓ	$\text{m}\cdot\text{s}^{-1}$	liquid velocity
\bar{u}_s	$\text{m}\cdot\text{s}^{-1}$	solid velocity
Δx	m	mesh size
ε	$\text{m}^2\cdot\text{s}^{-3}$	turbulence dissipation rate per unit of mass
λ	$\text{W m}^{-1}\cdot\text{K}^{-1}$	thermal conductivity
λ_{eff}	$\text{W m}^{-1}\cdot\text{K}^{-1}$	effective thermal conductivity due to turbulence
λ_t	$\text{W m}^{-1}\cdot\text{K}^{-1}$	turbulence thermal conductivity
λ_l	m	primary dendrite arm spacing
ρ	$\text{kg}\cdot\text{m}^{-3}$	density
μ_{eff}	$\text{kg}\cdot\text{m}^{-1}\cdot\text{s}^{-1}$	dynamic effective viscosity due to turbulence
μ_ℓ	$\text{kg}\cdot\text{m}^{-1}\cdot\text{s}^{-1}$	dynamic liquid viscosity
μ_t	$\text{kg}\cdot\text{m}^{-1}\cdot\text{s}^{-1}$	dynamic turbulence viscosity

REFERENCES

- [1] M. Rappaz, "Modelling of microstructure formation in solidification processes", *Intern. Mater. Rev.*, vol. 34, no. 3, pp. 93-123, 1989.
- [2] C. Beckermann, and R. Viskanta, "Mathematical modeling of transport phenomena during alloy solidification", *Appl. Mech. Rev.*, vol. 46, pp.1-27, 1993.
- [3] V.R. Voller, and C. Prakash, "A fixed grid numerical modeling methodology for convection – diffusion mushy region phase-change problems", *Int. J. Heat Mass Transfer*, vol. 30, No. 8, pp. 1709-1719, 1987.
- [4] V.R. Voller, A.D. Brent, and C. Prakash, "The modeling of heat, mass and solute transport in solidification systems", *Int. J. Heat Mass Transf.*, vol. 32, no. 9, pp. 1719-1719, 1989.
- [5] V.R. Voller, A.D. Brent, and C. Prakash, "Modeling the mushy region in a binary alloy", *Appl. Math. Model.*, vol. 14, pp. 320-326, 1990.
- [6] V.R. Voller, and C.R. Swaminathan, "general source-based method for solidification phase change", *Numer. Heat Transf., Part B*, vol. 19, pp. 175-189, 1991.
- [7] P.J. Prescott, and F.P. Incropera, "The effect of turbulence on solidification of a binary metal alloy with electromagnetic stirring", in: *Transport Phenomena in Materials Processing and Manufacturing*, ASME HTD, 1994, vol. 280, pp. 59-69.
- [8] P.J. Prescott, and F.P. Incropera, "convective transport phenomena and macrosegregation during solidification of a binary metal alloy: I-Numerical predictions", *J. Heat Transf.*, vol. 116, pp. 735-741, 1994.
- [9] P.J. Prescott, F.P. Incropera, and D.R. Gaskell, "Convective transport phenomena and macrosegregation during solidification of a binary metal alloy: II-Experiments and comparisons with numerical predictions", *Trans. ASME*, vol. 116, pp. 742-749, 1994.
- [10] P.J. Prescott, and F.P. Incropera, "The effect of turbulence on solidification of a binary metal alloy with electromagnetic stirring", *Trans. ASME*, vol. 117, pp. 716-724, 1995.
- [11] J.P. Gu, and C. Beckermann, "Simulation of convection and macrosegregation in a large steel ingot", *Metal. Mater. Trans. A*, vol. 33A, pp.1357-1366, 1999.
- [12] C. Pfeiler, B.G. Thomas, M. Wu, A. Ludwig, and A. Kharicha, "Solidification and particle entrapment during continuous casting steel", *Steel Res. Int.*, vol. 79, pp. 599-607, 2008.
- [13] M. Wu, A. Ludwig, C. Pfeiler, and F. Mayer, "multiphase flow modelling and its application potentials in steel continuous casting", *J. Iron Steel Res. Int.*, vol. 15 (Suppl 1), pp. 30-37, 2008.
- [14] B.G. Thomas, R. O'Malley, and D. Stone, "Measurement of temperature, solidification, and microstructure in a continuous cast thin slab", Proceedings of McWASP VIII, TMS Publications. Warrendale, Pennsylvania, US. 1998, pp. 1185-1198..
- [15] A.Nakayama, and F. Kuwahara, "Macroscopic turbulence model for flow in a porous medium", *J. Fluids Eng. – Trans. ASME*, vol. 121, pp. 427-433, 1999.
- [16] A.Nakayama, and F. Kuwahara, "A general macroscopic turbulence model for flows in packed beds, channels, pipes, and rod bundles", *J. Fluids Eng. – Trans. ASME*, vol. 130, pp. 1012051-1012057, 2008.
- [17] T. Masuoka, and Y. Takatsu, "turbulence model for flow through porous media", *Int. J. Heat Mass Transf.*, vol. 39, pp. 2803-2809, 1996.

Received: September 25, 2009

Revised: February 25, 2010

Accepted: February 26, 2010

© Wu et al.; Licensee Bentham Open.

This is an open access article licensed under the terms of the Creative Commons Attribution Non-Commercial License (<http://creativecommons.org/licenses/by-nc/3.0/>) which permits unrestricted, non-commercial use, distribution and reproduction in any medium, provided the work is properly cited.